Kazrin C entraps early endosomes at the pericentriolar region and facilitates endocytic recycling

Ines Hernandez-Perez[1], Adrian Baumann[1], Henrique Girao[1], Anna M. Aragay[1], Elena Rebollo[1] and Maria Isabel Geli[1,*]

[1]Institute for Molecular Biology of Barcelona (IBMB, CSIC), Baldiri Reixac 15, 08028 Barcelona, Spain.

*Correspondence: mgfbmc@ibmb.csic.es

ORCID: 0000-0002-3452-6700

Abstract

We identified kazrin C as a human protein that inhibits clathrin-mediated endocytosis when overexpressed. We now generated kazrin knock out and GFP-kazrin C expressing MEF lines to investigate in detail its function in endocytic traffic. We find that kazrin depletion delays recycling of internalized material and causes accumulation and dispersal of early endosomes (EE), indicating a role in transport from the early to the perinuclear recycling endosomes (RE). Consistently, we found that the C-terminal domain of kazrin C, predicted to be an intrinsically disordered region (IDR), specifically interacts with several endosomal components, including Epsin Homology Domain (EHD) proteins, γ-adaptin, and phosphatidyl-inositol-3 phosphate. Further, kazrin C shares homology with dynein/dynactin adaptors, it directly interacts with the dynactin complex and the dynein light intermediate chain LIC1, and overexpressed GFP-kazrin C forms condensates that entrap EE in the vicinity of the centrosome, in a microtubule-dependent manner. Altogether, the data indicates that kazrin C facilitates cargo recycling by trapping EE or EE-derived transport intermediates at the perinuclear region, where transfer of cargo to the RE might occur.

INTRODUCTION

Kazrin is a highly conserved and broadly expressed vertebrate protein, which was first identified as a transcript present in human brain (Kikuno et al., 1999). The human kazrin gene is located on chromosome 1p36.21 and encodes at least seven isoforms (A-F and K), generated by alternative splicing (Groot et al., 2004; Nachat et al., 2009; Wang et al., 2009). From those, kazrin C is the shorter isoform that constitutes the core of all other versions, which bear N or C-terminal extensions. Since its discovery, several laboratories have reported a broad range of roles for the different kazrin isoforms in a myriad of experimental model systems. Thus, in humans, kazrin participates in structuring the skin cornified envelope and promotes keratinocyte terminal differentiation (Groot et al., 2004; Sevilla et al., 2008a). In U373MG human astrocytoma cells, kazrin depletion leads to caspase activation and apoptosis (Wang et al., 2009). In Xenopus embryos instead, kazrin is important to maintain the ectoderm integrity and its depletion causes skin blisters, probably derived from defects in establishing cell-cell contacts (Sevilla et al., 2008b). In addition, depletion of kazrin causes craniofacial development defects, linked to altered Epidermal to Mesenchymal Transition (EMT) and migration of neural crest cells (Cho et al., 2011). The subcellular localization of kazrin recapitulates its functional diversity. Depending on the isoform and cell type under analysis, kazrin has been reported in association with desmosomes (Groot et al., 2004), adherens junction components (Cho et al., 2010; Sevilla et al., 2008a), the nucleus (Groot et al., 2004; Sevilla et al., 2008a), or the microtubule cytoskeleton (Nachat et al., 2009). At the molecular level, the N-terminus of kazrin directly interacts with several p120-catenin family members (Sevilla et al., 2008a) as well as with the desmosomal component periplakin (Groot et al., 2004), and it somehow regulates cell adhesion, as well as RhoA activity (Cho et al., 2010; Groot et al., 2004; Sevilla et al.,

2008a). How kazrin orchestrate such many cellular functions at the molecular level is far from being understood.

We previously identified human kazrin C as a cDNA that when overexpressed potently inhibits clathrin mediated endocytosis. In the present work, we generated MEF kazrin knock out for all kazrin isoforms (kazKO) and GFP-kazrin C expressing cells over the null MEF background (GFP-kazC) to analyze in detail its role in endocytic traffic. We found that depletion of kazrin causes accumulation of peripheral early endosomes (EE) and delays transfer of endocytosed transferrin to the perinuclear region where the recycling endosomes (RE) concentrate. Consequently, cellular functions requiring intact endosomal traffic through the REs, such as cell migration and cytokinetic abscission, were also altered. Consistent with its role in endocytic traffic, endogenous kazrin was detected on EE and its C-terminal domain interacted with different components of these organelles. Further, we found that the N-terminus of kazrin C shares homology with dynein/dynactin adaptors such as BICDR1 and Hook3 and that it directly interacts with the dynactin complex and the dynein intermediate chain LIC1, suggesting that it might work as an endosomal dynein adaptor. However, we found that that GFP-kazrin C does not extensively co-localize with EE but rather it forms condensates that trap these organelles in the vicinity of the centrosome in a microtubule-dependent manner. The data indicate that kazrin C is transported to the pericentriolar region by the dynein/dynactin complex where it facilitates transfer of endocytosed material from EE to RE by promoting the pericentriolar accumulation of EE or EE-derived transport intermediates.

RESULTS

Kazrin depletion impairs endosomal traffic

We originally identified kazrin C as a human brain cDNA whose overexpression causes the accumulation of the Transferrin (Tfn) Receptor (TfnR) at the plasma membrane (PM) in Cos7 cells (Schmelzl and Geli, 2002), suggesting that kazrin might be involved in clathrin-mediated endocytic uptake from the PM. However, depletion of kazrin using shRNA in Cos7 cells (Fig. S1A) did not significantly alter endocytic internalization but rather caused the accumulation of TxR-Tfn labeled peripheral endosomes (Fig. S1B), indicating a role of kazrin downstream in the pathway, possibly in endocytic traffic, either from the EE to the PM or from the EE to the perinuclear RE.

shRNA transfection in Cos7 cells did not achieved complete kazrin depletion in a reproducible manner. To overcome this problem, we generated kazrin knockout MEFs using the CRISPR CAS9 technology, and used a lentiviral system to subsequently create two cell lines that expressed GFP or GFP-kazrin C upon doxycycline induction (Fig S1C), allowing controlled kazrin C expression. Immunoblot analysis demonstrated that the expression level of GFP-kazrin C in the absence of doxycycline or upon a short o/n incubation was similar to the physiological level (low expression, 1 to 4 times the endogenous kazrin expression level) (Fig. S1D). Under these conditions, the GFP-kazrin C was not detectable by fluorescence microscopy. This might explain why none of the commercially available or home-made anti-kazrin antibodies detected a specific signal in wild type MEFs. Doxycycline incubation for longer periods (24 to 48 hours) resulted in moderate (4 to 8 times the endogenous kazrin expression levels) to high non-physiological GFP-kazrin C overexpression (more than 8 times the endogenous kazrin expression level) (Fig S1D), but allowed us to visualize its localization by microscopy (Fig. S1E).

In agreement with the Cos7 cell shRNA data, kazKO MEFs had an abnormal endosomal distribution, as compared to WT MEF, kazKO MEFs accumulating peripheral EEA1-

positive structures (Fig. 1A & B). The perinuclear distribution of the RE labeled with Rab11 was however not significantly affected in KazKO MEF (Fig. S1F). Low expression of GFP-kazrin C partially recovered the EEA1 perinuclear distribution, when compared to GFP (Fig. 1A & B). Consistent with a role of kazrin in endocytic traffic towards the perinuclear region, endocytosed TxR-Tfn accumulated in the periphery of kazKO cells after a 10 minute incubation, whereas it was found in the perinuclear region in most WT cells (Fig. 1C). Recycling of TxR-Tfn back to the PM was also significantly slower in kazKO cells (Fig. 1D), albeit traffic back to the surface was not completely blocked. A partial block in recycling was expected since the TfnR can be transported back to the PM following different pathways: a Rab4-dependent shortcut from peripheral EE, or a longer via that requires its traffic to the perinuclear RE, from where it is transported to the PM in a Rab11-dependent manner (Sheff et al., 2002). All endocytic trafficking defects were recovered by low expression of GFP-kazrin C but not GFP (Fig. 1A to E), indicating a direct role of kazrin in the process.

To further confirm the specific role of kazrin in endocytic recycling via the perinuclear RE, we analyzed its implication in cellular processes that strongly rely on this pathway, such as cell migration and invasion (Wilson et al., 2018). Analysis of the 3D migration of single WT and kazKO cells through Matrigel demonstrated that depletion of kazrin significantly diminished the migration speed, which was recovered upon re-expressing GFP-kazrin C at low levels, but not GFP (Fig. 2A & B, Movie 1). We also observed an increased persistency in kazKO cells (Fig. S2A), but it was not recovered with GFP-kazrin C re-expression (Fig. S2A). Increased persistency might be a secondary effect caused by the trafficking block to the RE, which might accelerate recycling via the shortcut circuit, as previously observed (Perrin et al., 2013; White et al., 2007). The long recycling circuit also

plays an important role in the last abscission step during cytokinesis (Pollard and O'Shaughnessy, 2019; Wilson et al., 2005). Consistent with kazrin playing a role in the long recycling circuit, kazKO cells had a significant delay in cell separation after cytokinesis, which was again partially restored by GFP-kazrin C expression (Fig. 2C and Movie 2).

Kazrin is recruited to EE and interacts with several components of the endosomal machinery.

Next, we investigated whether endogenous kazrin was present on EE. For that purpose, we used subcellular fractionation and immunoblot because the endogenous protein was not detectable by fluorescence microscopy, nor was GFP-kazrin C expressed at physiological levels. As shown in figure 3A, endogenous kazrin neatly co-fractionated with EE markers in the lightest fractions, such as the tethering factor EEA1 and the EHD proteins. On the contrary, it only partially co-fractionated with an early-to-late endosome marker (VPS35) and did not with markers of recycling endosomes (rab11) or the Golgi apparatus (GM130; Fig. 3A). Overexpressed GFP-kazrin C also co-fractionated with EE, although it appeared more spread in the gradient (Fig. 3A). Endogenous kazrin localization at EE was confirmed by subcellular fractionation experiments in Cos7 cells (Fig. S2B).

To confirm the interaction of kazrin C with endosomes, we immunoprecipitated GFP-kazrin C from native cellular extracts and probed the immunoprecipitates for a number of proteins involved in endosomal trafficking. Indeed, we detected specific interactions of GFP-kazrin C with EHD proteins, as well as with clathrin and γ-adaptin, a component of the Golgi and endosomal clathrin adaptor AP-1 (Fig. 3B). No interaction with the retromer subunit Vps35, the tethering factor EEA1, or the clathrin adaptors GGA2 or AP-2 could be demonstrated in immunoprecipitations assays (Fig. 3B), indicating that kazrin C might

preferably bind the machinery implicated in endosomal traffic from early to or through REs (Grant and Caplan, 2008; Perrin et al., 2013). Pull down assays with purified components indicated that kazrin C can directly interact with EHD1 and EHD3, with a slight preference for EHD3, the clathrin terminal domain and the γ-adaptin ear. The interaction with γ-adaptin seemed to be the strongest (Fig. 3C). Using pull down assays with purified truncated versions of kazrin C, we mapped the γ-adaptin binding domain within the C-terminal half of the protein, predicted to be an intrinsically disordered region (IRD) (Fig. 3D & S2C). The interaction of endogenous kazrin with γ-adaptin and clathrin could also be confirmed in co-immunoprecipitation experiments from Cos7 and MEFs, using a polyclonal antibody raised against the C-terminus of purified kazrin C (Fig. S2D). Also consistent with kazrin specifically interacting with EE, we found that, purified kazrin C specifically interacted with phosphatidyl-inositol-3-phosphate (PI3P) (Fig. 3E), a lipid particularly enriched on EE (Wang et al., 2019). The interaction required the polyK stretch in the C-terminus of kazrin C (Fig. 3E), previously proposed to constitute a nuclear localization signal (Groot et al., 2004).

Kazrin C localizes at the pericentriolar region and directly interacts with dynactin and LIC1.

In an effort to visualize a link between kazrin and the EEs, we imaged the subcellular localization of moderately overexpressed GFP-kazrin C. Under these conditions, the previously reported localization of kazrin C in the nucleus and at cell-cell contacts was evident (Fig. S3A; (Groot et al., 2004)). At the PM and some internal vesicle-like structures, GFP-kazrin C neatly co-localized with the adherens junction components N-cadherin, β-catenin and p120-catenin, but not with desmoglein (Fig. S3A). However, despite we detected limited co-localization of GFP-kazrin C with EHD tubules and

peripheral γ-adaptin structures (Fig. S3B), we failed to demonstrate extensive co-localization between EEA1 and GFP-kazrin C (Fig. 4A), indicating that GFP-kazrin C only transiently interacted with EE or it did with certain endosomal subdomains or endosomal subpopulations. Interestingly though, we observed that GFP-kazrin C appeared in two bright circular structures that co-localized or appear in close apposition with pericentrin (Fig. 4B) and that seem to entrap EE (Fig. 4A). Live-cell imaging evidenced small GFP-kazrin C condensates moving in and out from the pericentriolar region (Fig. S3B, Movie 3). These structures were reminiscent of pericentriolar satellites, which are IDR-enriched membrane-less compartments that transport centrosomal components in a microtubule-dependent manner (Prosser and Pelletier, 2020). Transfection of MEF overexpressing GFP-kazrin C with the EE marker Rab4-mCherry further evidenced the formation of condensates, mostly pericentriolar, which entrapped enlarged endosomes (Movie 4 to 6 and Fig. S4). Treatment with nocodazole disrupted the centrosomal localization of GFP-kazrin C, as well as the concomitant perinuclear accumulation of EE (Fig. 4C & D), indicating that EE and GFP-kazrin C localization at the pericentrosomal region required minus end directed microtubule-dependent transport, mostly effected by the dynactin/dynein complex (Flores-Rodriguez et al., 2011).

Our observations indicated that kazrin C can be transported in an out the pericentriolar region along microtubule tracks. Also, the pericentriolar localization of GFP-kazrin C was reminiscent of that observed for well-established or candidate dynein/dynactin activating adaptors such as Hook2 or Hook3 (Baron and Salisbury, 1988; Szebenyi et al., 2007). Further, we found that kazrin C shared 23.3% identity and 57.3 % similarity with BICDR1 (Fig. 4E) over 232 amino acids, and 19.6% identity and 61.3 % similarity with Hook3 over 168 amino acids, in the range of the homology between Hook3 and BICDR1 (24.7%

identity and 56.7 % similarity over 268 amino acids) (LALIGN). Therefore, we hypothesized that kazrin might also interact with the dynein/dynactin complex. Consistent with this hypothesis, we found that moderately expressed GFP-kazrin C, over a kazKO background, pulled-down the dynactin component p150glued from cell extracts, whereas GFP alone did not (Fig. 4F). Similar to what had been described for other dynein/dynactin adaptors (Kendrick 2019 JCB), we also detected co-immunoprecipitation of GFP-kazrin C with kinesin-1 (Fig. 4F). We observed no co-immunoprecipitation with tubulin (Fig. 4F), indicating that GFP-kazrin C interactions with dynactin and kinesin-1 were not indirectly mediated by microtubules. Pull down experiments with GST-kazrin C expressed and purified from *E. coli* and the dynactin complex purified from pig (Jha et al., 2017) demonstrated that the interaction was direct and that it was contributed by both the N- and C-terminal halves of kazrin C (Fig. 4G), suggesting multiple contacts with different dynactin components. As also described for other dynein/dynactin adaptors such as BICD2, CRACR2a and HOOK3 (Lee et al., 2020), pull down experiments with purified components evidenced a weak, albeit specific interaction of kazrin C with the dynein Light Intermediate Chain 1 LIC1, but not with LIC2 (Fig. 4G). Finally, immunoprecipitation experiments from MEFs using a polyclonal antibody against the C-terminus of kazrin C also indicated binding of endogenous kazrin with the dynactin complex (Fig. 4E).

Discussion

Our data demonstrates the kazrin plays a direct role in endosomal recycling through the long pathway traversing the perinuclear region. We show that endogenous kazrin is recruited to EE and directly interacts with several EE components that have been implicated in this process (Grant and Caplan, 2008; Perrin et al., 2013). Further, depletion of kazrin causes a defect in the transfer of endocytosed Tfn to the perinuclear region and

the scattering of EE to the cell periphery, similar to what is observed when depleting other proteins involved in EE to RE transport such as EHD3, or upon inhibition of dynein (Driskell et al., 2007; Naslavsky et al., 2006; Nielsen et al., 1999).

While the vesicular nature of membrane traffic from the PM to the EE has been well characterized, the principles governing the transport of cargo within the endosomal system are much less understood. The more accepted view is that the core of the EE, receiving the internalized material, undergoes a maturation process that leads to its conversion to LE, while retrograde traffic is driven by tubular transport intermediates, generated by sortinexins (SNX) or clathrin coated vesicles (Haberg et al., 2008; Hsu et al., 2012; McNally and Cullen, 2018). The diversity of sortinexins and clathrin adaptors reflects the diversity of tubulo-vesicular structures that emanate from distinct endosomal subdomains, which retrieve specific cargo and presumably pour their content to different acceptor compartments. However, alternative models have been proposed, where the centripetal transport of EE to the pericentriolar region facilitates fusion with or maturation to RE (Naslavsky and Caplan, 2018; Solinger et al., 2020).

Within this wide range of processes, microtubules play key roles. EEs move along microtubule tracts with a bias toward the cell center (Driskell et al., 2007; Nielsen et al., 1999). Centripetal movement is mainly effected by the dynein/dynactin complex, whereas kinesins bring the organelles to the cell periphery (Granger et al., 2014). Treatment of cells with nocodazol or interfering with dynein results in inhibition of endosome motility, the scattering of EE to the cell periphery and impaired endosomal maturation (Granger et al., 2014). In addition, plus and minus end directed microtubule-dependent-motors have both a role in maintaining the endosomal subdomain organization and in the formation and motility of SNX-dependent tubular structures (Granger et al., 2014).

Interestingly, motility of different SNX tubules or subdomains is associated with distinct dynein complexes bearing either the LIC1 or LIC2 chains and particular kinesin types (Hunt et al., 2013). In this context, the interactome of kazrin C suggests that it might work as a LIC1-dynein and kinesin-1 adaptor for EHD and/or AP-1/clathrin transport intermediates emanating from EE, in transit to the RE (Grant and Caplan, 2008; Perrin et al., 2013). The limited localization of GFP-kazrin C with peripheral structures decorated with EHD and γ-adaptin, indeed suggests that kazrin associates with a subset of endosomal transport intermediates, maybe specialized in the recycling of adherens junction components. However, this sole kazrin endocytic function could hardly explain the broader effects on the Tfn recycling and on the EE distribution, observed upon its depletion. In this context, we observed that GFP-kazrin C moves in and out from the pericentriolar region, where it forms condensates that entrap EE, suggesting a model whereby kazrin C travels to the pericentriolar region as passive cargo for dynein and once there, it forms condensates that entraps EE or EE-derived transport intermediates in the vicinity of the RE, to facilitate tethering and eventually fusion. The loosely structured kazrin C IDR bearing multiple EE binding sites could form the trapping mesh, while the dynein/dynactin adaptor homology regions would hook kazrin C directly to dynein for its own transportation and/or compete with other EE adaptors to facilitate unloading in the vicinity of the centrioles.

The role of kazrin in endocytic recycling, might explain some of the pleiotropic effects observed in vertebrate development upon depletion of different kazrin isoforms. Defects in the establishment of cell-cell contacts in Xenopus embryos and human keratynocytes (Cho et al., 2010; Sevilla et al., 2008a; Sevilla et al., 2008b) might derive from altered recycling of cadherins or desmosomal components (Kawauchi, 2012). Likewise, eye and craniofacial defects in kazrin depleted Xenopus embryos, associated with reduced neural crest migration

(Cho et al., 2011), might as well be ultimately caused by altered endocytic trafficking of integrins, cadherins or receptor tyrosine kinases, among others (Jones et al., 2006).

MATERIALS AND METHODS

DNA techniques and plasmid construction. Oligonucleotides used for plasmids construction and information about the construction strategies are available upon request. DNA manipulations were performed as described (Sambrook et al., 1989), or the Getaway cloning system (Life Technologies) in the case of lentiviral vectors. Enzymes for molecular biology were obtained from New England Biolabs. Plasmids were purified with the Nucleospin plasmid purification kit (Macherey-Nagel). DNA was purified from agarose gels using the gel extraction kit from Qiagen. PCRs were performed with the Expand High Fidelity polymerase (Roche) and a TRIO-thermoblock (Biometra GmbH). Plasmids used are listed in Table I.

Cell culture and cell line establishment. Cos7 cells were obtained from the DSMZ. MEF and HEK293T cells were provided by A. Aragay (IBMB-CSIC). Cells were grown in DMEM (Thermo Fisher) supplemented with 10 % FCS, 100 µ/ml penicillin, 100 µg/ml streptaminicin and 2 mM L-glutamine (Thermo Fisher) in a humidified 5 % CO_2 atmosphere at 37°C. Cos7 were transiently transfected with Lipofectamine 2000 (Thermo Fisher). Cells were analyzed 24 h after transfection. For shRNA kazrin depletion, pKLO.1_shKaz from Sigma Mission Library 2007 (Clone ID TRCN000018283) was used. pLKO.1_CV/_SCR (SHC002) was used as a control. For lentivirus production and Cos7 cells transfection, HEK293**T** cells were co-transfected with either the pLL3.7 encoding GFP, for virus production control and infection efficiency monitoring, or with pLKO.1 encoding the desired shRNA, and the viral packaging (pCMV-dR8.2 dvpr) and envelope (pCMV-VSV-G) plasmids, using calcium phosphate transfection (see chapter 7.2.2). About

16 hours after transfection, the medium was changed and half of the usual volume was added. During the two following days, medium containing the virus was collected and filtered with a 0.45 µm filter (Millipore). The filtered virus solution was directly used for the infection of cell lines or stored in aliquots at -80°C without prior concentration of the virus. Infection and selection of stably infected cells were done in the presence of the appropriate concentration of puromycin (Sigma-Aldrich) titrated by using the minimum antibiotic concentration sufficient to kill untransfected cells, but to maintain cells transfected with the pLL3.7 GFP-containing plasmid. Actual depletion of kazrin or the protein of interest was analyzed by immunoblot (see chapter 7.3.1).

MEF KO cells were produced with the CRISPR-CAS9 system. Two guide RNAs were design to recognize regions at the start of exon 2 of the kazrin gene, corresponding to the start of kazrin C isoform (CACCGAATGCTGGCGAAGGACCTGG and CACCGCCTTCTGTACCAGCTGCACC). Online tools Benchling (https://www.benchling.com/) and the Broad Institute tool GPP (https://portals.broadinstitute.org/gpp/public/analysis-tools/sgrna-design) were used for the design. Guide RNA oligonucleotides were annealed and inserted into a pSpCas9(BB)-2A-GFP pX458 vector. MEFs were electroporated with Nucleofector (Lonza) following the manufacturer's instructions. GFP-positive cells were sorted by FACS in an Aria FUSION (Becton Dikinson) sorter and screened by immunoblotting with antibodies against the N-terminal and the C-terminal part of kazrin. Lentiviral particles were produced in HEK 293T cells. Calcium phosphate-mediated transfection was used to deliver vector pINDUCER20 containing GFP or GFP-tagged kazrin constructs, together with packaging and envelope lentiviral vectors. The supernatant of transfected HEK 293T cells was collected after 16 h, 0.45 mm-filtered and added to MEFs. The cells were passaged for a week, incubated with 5

µg/ml doxycycline hyclate (Millipore) for 48 h to induce the expression of the construct. GFP-positive cells were selected by FACS and pooled. To study the effect of microtubule dynamics, MEFs were treated with 100 ng/ml of nocodazole (Sigma) or DMSO for 16 h, then fixed at room temperature. MEFs were transfected by electroporation using the Ingenio solution (Mirus) and a nucleofector (Amaxa). The cells were processed 2 days after electroporation.

TxR-Tfn uptake and recycling assays. Cos7 or MEFs were grown on R-collagen-coated glass coverslips. For uptake experiments, cells were starved for 30 min in DMEM without FBS or BSA. Cells were incubated with pre-warmed DMEM containing 20 µg/ml of TxR-Tfn (from human serum, Molecular Probes) and 0.1 % BSA for the specified times. Cells were washed in ice-cold PBS once and fixed in 4 % PFA (Sigma) for 20 min on ice. The effect on CME in Cos7 cells was determined by scoring cells showing normal, reduced or no uptake of TxR-Tfn. In MEFs, individual cells were delimited with the free hand drawing tool in Fiji. The mean fluorescence signal per cell was quantified and the mean cytosolic background in each cell was subtracted to that value. TxR-Tfn perinuclear enrichment in MEFs was the signal within a 10 µm diameter circle in the perinuclear region divided by the signal in the whole cell.

For recycling experiments, cells were starved for 30 min in DMEM without FBS. 20 µg/ml of TxR-Tfn in DMEM with 0.1 % BSA was added on ice. Plates were incubated at 16 °C for 30 min, then washed in ice-cold PBS with 25 mM acetic acid pH 4.2 and with PBS. Cells were incubated in 500 µg/ml unlabeled Tfn (Sigma) in DMEM with 0.1 % BSA at 37 °C, then transferred to ice at different time points, washed in ice-cold PBS with 25 mM acetic acid pH 4.2 and with PBS. They were fixed in 4 % PFA for 20 min on ice. Individual cells were delimited with the free hand drawing tool in Fiji. The threshold of the images

was adjusted to create a mask in which only endosomal Tfn was included, excluding the cytosolic signal, then the mean intensity per cell was measured. Images were taken with a Zeiss LSM780 confocal microscope.

Immunofluorescence. Cells were seeded onto cover-glasses and fixed with 4 % PFA in PBS containing 0.02 % BSA and 0.02 % sodium azide (PBS*), for 10 min at room temperature. Cells were washed 3 times for 5 min with PBS* and permeabilized with PBS* containing 0.25 % Triton X-100 for 10 min. Cells were washed 3 times for 5 min with PBS* and incubated for 20 min in PBS* containing 1 % BSA. Cells were then incubated in the presence of the primary antibody in PBS* for 1 h at room temperature, washed 3 times with PBS* and incubate for 1 h in the presence of the secondary antibodies prepared in PBS*. Cells were washed 3 times with PBS* and mounted using Prolong that included DAPI for nuclear staining (Thermo Fisher). Images were taken with a Zeiss LSM780 confocal microscope.

Perinuclear enrichment of EEA1 and rab11 in MEFs was the integrated density within a 10 µm diameter circle in the perinuclear region divided by the integrated density in the whole cell as delimited with the free hand drawing tool in Fiji.

Cell migration and division assays. Cells were plated on 400 µg/ml Matrigel (Corning)-coated plates at low density and incubated for 5 h. Once the cells were attached, the medium was replaced by Matrigel for 30 min to embed the cells in a matrix. Matrigel excess was then removed and cells were kept at 37 °C with 5 % CO_2 during imaging. Phase contrast images were taken every 10 min for a total of 13 h in a Leica AF700 microscope with a 10x objective. To analyse cell migration, cells were tracked using the Fiji plugin MTrackJ and the speed and directionality calculated with the program DiPer (Gorelik and Gautreau 2014). The duration of late telophase and cytokinesis during cell division was

measured from the moment daughter cells attach to the substrate until they completely detach from each other.

Live confocal imaging. Cells were seeded on plates with polymer coverslips for high-end microscopy (Ibidi). 5 µg/ml of doxycycline was added for 24 h before imaging for visualization of GFP-kazrin C. Cells were kept at 37°C with 5 % CO_2 during the imaging. Images were taken every 2.65 s on a Zeiss LSM780 confocal microscope.

Microscope specifications. Epifluorescence images were taken on a Leica DMI6000 wide-field microscope equipped with a 10x objective, a Hamamatsu Orca-R2 camera and a SOLA-SMII white LED illumination source. The system was controlled under the LAS X (Leica Application Suite X) software. Confocal images were taken on a Zeiss LSM-780 confocal microscope system was equipped with a diode laser (405 nm), multiline argon laser (458/488/514 nm), solid state DPSS Laser (561 nm), HeNe laser (594 nm) and HeNe laser (633 nm). The objective used was a 63x/1.4NA oil DIC Plan-Apochromat objective. The internal detectors of the LSM-780 system had three channels, two usual PMTs (photomultiplier tubes) and a 32 PMT GaAsP array that can be used for photon counting, all PMTs usable for fluorescence and reflection and an additional PMT for transmitted light, allowing simultaneously detection of fluorescence and bright field images. The system was controlled with the LSM software Zen2.1.

SDS-PAGE and immunoblots. SDS–PAGE was performed as described (Laemmli, 1970) using pre-casted Mini-PROTEAN TGX 4-20% Acrylamide gels (Bio Rad). Protein transfer, blotting and chemiluminescence detection were performed using standard procedures. Detection of proteins was performed using the ECL kit (GE Healthcare).

Optiprep gradient cell fractionation. Performed as described in Li and Donowitz (2014). Briefly, cells were scraped from the plate, harvested by centrifugation at 700 g for 10 min

and resuspended in 1 ml of ice cold Lysis buffer (LB: 25 mM Hepes pH 7.4, 150 mM NaCl, 1 mM DTT, 2 mM EGTA) containing protease inhibitors. The cell suspension was then passed 10 times through a 27 G needle. The lysate was cleared by centrifuging twice at 3,000 g for 15 min. The supernatant was subsequently centrifuged at 186,000 g for 1 h at 4 °C to fractionate cellular membranes from cytosol. The membrane pellet was resuspended in LB with protease inhibitors, passed 10 times though a 27 G needle and laid on an Optiprep (Sigma) gradient. A 12 ml 2 % step Optiprep gradient in LB ranging from 32 % to 10 % was prepared beforehand in Ultra-Clear tubes (Beckman Coulter). Samples were spun for 16 h at 100,000 g at 4 °C. 0.6 ml fractions were carefully collected from the top. Samples were then precipitated with trichloroacetic acid, air-dried and resuspended in SDS-PAGE sample buffer for immunoblot analysis.

GST pull downs, GFP-trap and endogenous immunoprecipitations. Purification of recombinant GST and 6-His fusion proteins from BL21 *E. coli* (Novagen) was performed as described (Geli et al, 2000). Pull down experiments were performed with GSH beads (GE Healthcare) coated with 0.5 µg of the indicated GST-tagged proteins and 2nM of eluted 6xHis-kazrin C or 2 nM of the dynactin complex, incubated in 1 ml of binding buffer containing PBS, 0.1 % Triton-X100 and 0.5 % BSA with protease inhibitors (Complete Roche) for 1 h at 4 °C in a head-over-shoulder rotation. Beads were washed three times with PBS-Tween, twice with 1 ml of PBS with 0.1 % Triton X-100 and once with 1 ml of PBS-Triton with 0.5 % BSA. The beads were boiled in Laemmli buffer. Input and pull down samples were loaded in an SDS-PAGE gel and analysed by immunoblot.

For immunoprecipitations from GFP and GFP-kazrin C overexpressing MEFs, the cells were seeded in the presence of 5 µg/ml of doxycycline on the day before the experiment. The cells were harvested and cleared at 100 g. The pellet was resuspended in 500 µl of IP

buffer (20 mM Hepes, 50 mM KAc, 2 mM EDTA, 200 mM sorbitol, 0.1 % Triton X-100, pH 7.2) containing protease inhibitors and passed 30 times through a 27 G needle. The lysate was cleared by centrifuging 5 min at 10,000 g. The protein concentration of the samples was adjusted. 10 µl of GFP-binding agarose beads (Chromotek) were incubated with the protein extract for 1 h at 4 ºC in head-over-shoulder rotation. Beads were washed six times with 1 ml of IP buffer. The beads were boiled in Laemmli buffer. Input and IP samples were loaded in an SDS-PAGE gel and analysed by immunoblot.

For endogenous immunoprecipitations, WT or kzKO cell extracts were generated as described above but incubated with rabbit IgGs against the kazrin C C-terminus (aa 148 to 327), pre-bound from a serum to Protein A-Sepharose or IgGs from the pre-immune serum.

Lipid strip assays. Lipid strips (Echelon) were incubated in 1 % skimmed milk in PBS for 1 h at room temperature. The corresponding GST fusion protein was added to a final concentration of 15 µg/ml in incubation buffer 10 mM Tris pH 8.0, 150 mM NaCl, 0.1 % Tween-20, 3 % BSA (fatty acid free, Sigma), with protease inhibitors overnight at 4 °C. The strips were washed three times for 10 min in the incubation buffer and developed by immunoblot.

Quantification and statistical analysis. Quantifications were performed with ImageJ (Rasband, WS, NIH, Bethesda, Maryland, USA, http://imagej.nih.gov/ij, 1997-2016). Statistical analysis was performed with GraphPad Prism. The D'Agostino-Pearson test was applied to data sets to assess normality. If the data followed a normal distribution or the result of the normality test was not significant, an unpaired two-tailed t test was performed to assess significance. If the distribution was not normal, a two-tailed Mann-Whitney test was used. Results are expressed as mean ±SEM with respect to the number of cells (n) for a representative experiment.

Prediction of intrinsically disordered regions was achieved with the IUPred2A software, which assigns each residue a IUPred score that is the probability of it being part of a IDR (Mészáros, Erdös and Dosztányi, 2018).

Antibodies. Polyclonal sera against kazrin for immunoblotting were generated in rabbit using an N-terminal (aa 1 to 147) and a C-terminal (aa 148 to 327) fragment of kazrin C fused to GST. Affinity purification of the serum against the N-terminus of kazrin C was performed using an active ester agarose (Affi-Gel, Bio-Rad) covalently link to the N-terminal fragment of kazrin C. The following commercial antibodies were used in this study: anti-rab11 (610656), anti-rab4 (610888), anti-rabaptin-5 (610676), anti-GM130 (610822), anti-GGA2 (612612), anti-clathrin heavy chain (610499), anti-p150 Glued (610473), anti-α-adaptin (610501), anti-γ-adaptin (610386), anti-N-cadherin (51-9001943), anti-β-catenin (610153), anti-p120-catenin (51-9002040) and anti-desmoglein (51-9001952) from BD Biosciences, anti-pericentrin (4448) and anti-EHD1 (109311) from Abcam, anti-VPS35 (374382) and anti-kinesin-1 heavy chain (133184) from Santa Cruz Biotechnology, anti-EEA1 (3288) from Cell Signalling Technology, anti-tubulin (T-6557) from Sigma, anti kazrin C (ab74114) from Abcam, anti-GFP (632380) from Living Colors and anti-GST (27-57701) from Amersham. Peroxidase-conjugated anti-mouse (A2554), anti-goat (A4174) and rabbit (A0545) IgGs were from Sigma. Alexa Fluor 568 anti-mouse IgG (A11037), Alexa Fluor 568 anti-rabbit IgG (A11036) and Alexa Fluor 647 anti-rabbit IgG (A21245) from Thermo Fisher.

Table I. Plasmids

Plasmid	Insert	Backbone

pGEX-5X-3	GST	pGEX-5X-3
pGST-hB24	GST + kazrin C, human gene KIAA1026	pGEX-4T-2
pGST-KazrinC(161-250)	GST + kazrin C-Ct minus polyK and acidic (aa 161-250)	pGEX-5X-3
pGST-kaz-Ct(251-327)	GST + kazrin C Ct (aa 251-327)	pGEX-5X-3
pGST-kaz-Ct(289-327)	GST + kazrin C Ct (aa 289-327)	pGEX-5X-3
pGST-kaz-Ct(161-327)	GST + kazrin C Ct (aa 161-327)	pGEX-5X-3
pGST-kaz-Ct(167-327)	GST + kazrin C Ct (aa 167-327)	pGEX-5X-3
pGST-kaz-Ct(148-327)	GST + kazrin C Ct (aa 148-327)	pGEX-5X-3
pGST-kaz-Ct(71-327)	GST + kazrin C Ct (aa 71-327)	pGEX-5X-3
pGST-kaz-Ct(1-294)	GST + kazrin C Ct (aa 1-294)	pGEX-5X-3
pGST-kaz-Ct(1-250)	GST + kazrin C Ct (aa 1-250)	pGEX-5X-3
pGST-kaz-Ct(1-176)	GST + kazrin C Ct (aa 1-176)	pGEX-5X-3
pGST-kaz-Ct(1-148)	GST + kazrin C Ct (aa 1-148)	pGEX-5X-3
pGST-kaz-Ct(1-70)	GST + kazrin C Ct (aa 1-70)	pGEX-5X-3
pGST-kaz-Ct-KA	GST + kazrin C Ct (aa 161-327) -(281-KRKKKK-286, AAAAAA)	pGEX-5X-3
pQE11-kazrin	6xHis + kazrin C	pQE11
pGST-EHD1	GST + EHD1	pGEX-5X-3
pGST-EHD3	GST +EHD3	pGEX-5X-3
pGST-γ-Adaptin-ear	GST + human AP1 Adaptin G1 ear (aa 702-925)	pGEX-5X-3
pGST-CHC17-TD	GST + human CHC17-aa1-483 (CHC TD + linker)	pGEX-5X-3
pGST-LIC1	GST + dynein light intermediate chain 1	pGEX-5X-3
pGST-LIC2	GST + dynein light intermediate chain 2	pGEX-5X-3
pX458-kaz KO 1	Cas9 and cas9 target sequence 1	pSpCas9(BB)-2A-GFP (pX458)

pX458-kaz KO 2	Cas9 and cas9 target sequence 2	pSpCas9(BB)-2A-GFP (pX458)
pVSV-G	Lentivirus envelope protein	pLenti-CMV
pAX8	Lentivirus packaging protein	pLenti-CMV
pINDUCER-EGFP	EGFP	pINDUCER20
pINDUCER-EGFP-kazrin	EGFP + kazrin C	pINDUCER20
pKLO.1_shKaz	cloneID TRCN00001 82832	pLK0.1
pLK0.1	SHC002	pLK0.1
pCMV-dR8.2dvpr		
pCMV-VSG-G		

Acknowledgements. M. Martínez for lentiviral plasmids and J. Roig for CRISPR plasmids. M. Robinson for sending the construct of the γ-adaptin ear fused to GST. and M. Mapelli for the GST-LIC1 and LIC2 constructs. T. Surrey and C. Mitchel for sharing the porcine purified dynactin complex. This work was financed by BFU2017-82959-P to MIG, BES-2012-053341 to AB and BES-2015-071691 to IHP, from the Spanish government.

FIGURE LEGENDS

Figure 1. Kazrin depletion impairs endosomal traffic. (A) Confocal images of WT, kazKO, GFP or GFP-kazrin-expressing MEFs, fixed and stained with an α-EEA1 antibody. Magnified insets showing endosomes in the peripheral areas for each cell type are shown on the right. Scale bar, 10 µm. Cell borders are indicated with dashed line and the nuclei in blue. (B) Graphs of mean ± SEM EEA1 perinuclear enrichment. The signal within a circle of 10 µm in the perinuclear region was quantified and divided by the total EEA1 signal in the cell. The values were normalised to the corresponding KO cells (either kazKO or GFP). The p values of a two-tailed Mann-Whitney test are shown. (C) On the left, confocal

images of the indicated MEFs incubated with TxR-Tfn for 0 min or 10 min. Scale bar, 10 μm. On the right, graphs of mean ± SEM TxR-Tfn perinuclear enrichment after a 10 min incubation with 20 μg/ml TxR-Tfn in the same cells. Cell borders are indicated by dashed and the nuclei in blue. The signal within a circle of 10 μm in the perinuclear region was quantified and divided by the total signal in the cell. The values were normalised to the corresponding KO cells (either kazKO or GFP). The p values of a two-tailed Mann-Whitney test are shown. (D) Graph of mean ± SEM TxR-Tfn signal in WT, kazKO, GFP and GFP-kazrin C-expressing MEFs in a recycling assay. Cells were incubated 30 min with 20 μg/ml TxR-Tfn at 16ºC to allow accumulation of cargo in EEs, washed and incubated with non-labelled Tfn at 37ºC to allow recycling. The cells were transferred to ice to stop recycling at different time points. The p values of a two-tailed t test comparing WT and kazKO samples or GFP and GFP-kazrin C expressing cells are shown.

Figure 2. Kazrin depletion impairs cell migration and division. (A) Plots of the paths described by individually migrating WT, kazKO, GFP and GFP-kazrin C-expressing MEFs. GFP and GFP-kazrin C MEFs were treated with 5 μg/ml doxycycline for 24 h before the start of the experiment. The cells were embedded in Matrigel and tracked for 9 h. All tracks start at the (0,0) coordinate in the graph. (B) Graphs of mean ± SEM speed of the cells described in (A). The data was normalized to the corresponding KO cells (either kazKO or GFP). The p values of two-tailed Mann-Whitney tests are shown. (C) Time lapse epifluorescence images of WT, kazKO, GFP-expressing and GFP-kazrin C-expressing MEFs embedded in Matrigel, as they divide. GFP and GFP-kazrin C MEFs were treated with 5 μg/ml doxycycline for 12 h before staring the experiment. (D) Graph of the mean ± SEM time lapse between substrate attachment and complete cell separation of the cells

described in (C). The data was normalized to the corresponding KO (kazKO or GFP). The p values of two-tailed Mann-Whitney tests are shown.

Figure 3. Kazrin is an endosomal protein. (A) Left, immunoblots of an Optiprep density gradient fractionation of membrane lysates of WT, kazKO and GFP-kazrin C-expressing cells. The membranes were probed with a rabbit polyclonal antibody against the kazrin C N-terminus, α-EEA1 and α-EHD1 (EE marker), α-VPS35 (rab5/rab7 transition endosomal marker), rab11 (RE marker), GM130 (*cis*-Golgi marker) and BIP (ER marker). Right, graph of the band intensities per fraction for kazrin or the indicated intracellular membrane markers. The signal intensities of each fraction were normalized to the maximum for each antibody. All gradients were loaded with the same amount of total protein. (B) Immunoblots of α-GFP agarose precipitates from GFP or GFP-kazrin C-expressing MEF cell lysates, probed with an α-EHD, α-EEA1, α-VPS35, α-rab4, α-rabaptin-5, α-Clathrin Heavy Chain (CHC), α-GGA2, α-α-adaptin, α-γ-adaptin and α-GFP antibodies. The cells were treated with 5 μg/ml doxycycline for 24 h before lysis. 10 μg of total protein were loaded as input. (C) Immunoblots of pull-downs with purified 6xHis-kazrin C incubated with GST, GST-EHD1, GST-EHD3, GST-Clathrin Heavy Chain terminal Domain (CHC-TD) or GST-γ-adaptin. The membranes were probed with an α-kazrin antibody (ab74114, from Abcam) or stained with Ponceau red (as a loading control). (D) Immunoblots of pull-downs with purified γ-adaptin ear, incubated with GST constructs fused to different portions of kazrin C including the indicated amino acids. The membranes were probed with a α-γ-adaptin antibody or stained with Ponceau red (as a loading control). A scheme with the kazrin C truncations used and their relative binding to γ-adaptin is shown on the right. (E) Immunoblots of a lipid binding assay performed with either purified GST-kazrin C C-terminal portion (amino acids 161-327) or an equivalent construct in which the poly-K

region has been mutated to poly-A, used as a control. The membranes used in this assay contain a concentration gradient of the indicated phosphoinositides. Membranes were probed with an anti-GST antibody.

Figure 4. Kazrin traps EE at the pericentriolar region. (A) Merged confocal images of GFP-kazrin-expressing MEFs, treated with 5 µg/ml doxycycline for 24 h before fixation and stained with an α-EEA1 antibody and a A568-conjugated secondary antibody. Individual channels and merged confocal images of 6x magnifications are shown. Scale bar, 10 µm. (B) Merged and individual channels confocal images of GFP or GFP-kazrin-expressing MEFs, treated with 5 µg/ml doxycycline for 24 h before fixation, and stained with a α-pericentrin antibody and a A568-conjugated secondary antibody. 3.5x magnifications are shown. Arrowheads indicate cell-cell borders. Scale bar, 10 µm. (C) Confocal images of GFP-kazrin-expressing MEFs, treated with 5 µg/ml doxycycline for 24 h and with DMSO or 100 ng/ml nocodazole for 16 h before fixation, and stained with an α-EEA1 antibody and a A568-conjugated secondary antibody, and DAPI. Scale bar, 5 µm. (D) Graphs of percentage ± SEM of cells with a perinuclear localization pattern of GFP-kazrin C (left) and graph of mean ± SEM EEA1 perinuclear enrichment (right) in cells treated as described in C. The EEA1 perinuclear enrichment was quantified as the signal within a circle of 10 µm in the perinuclear region divided by the total cell signal. The p values of a two-sided Fisher's exact test (left) and a two-tailed t test (right) are shown. **(**E) Sequence comparison between kazrin C and human BICDR1 calculated with LALIGN. (F) Immunoblots of α-GFP agarose immunoprecipitates (IP) from GFP-expressing or GFP-kazrin C-expressing MEF cell lysates, probed with an α-p150 glued (dynactin), α-kinesin-1, α-tubulin or α-GFP antibodies. The cells were treated with 5 µg/ml doxycycline for 24 h before lysis. (G) Immunoblots of pull-downs with purified GST, GST-tagged kazrin C full-

length, N-terminal portion (aa 1-176) or C-terminal portion (aa 161-327), incubated with (+) or without (-) the purified dynactin complex. The membranes were probed with an α-p150 glued or stained with Ponceau red (as a loading control). (H) Immunoblots of pull-downs with purified 6xHis-kazrin C incubated with GST, GST-LIC1 or GST-LIC2. The membranes were probed with an α-kazrin antibody or stained with Ponceau red (as a loading control). (I) Immunoblot of protein A-Sepharose immunoprecipitates (IP) from WT or kazKO MEFs using a mix of rabbit polyclonal serums against the N and C-terminal domains of kazrin C or a pre-immunisation serum, probed with an α-p150 glued (dynactin) antibody.

Bibliography

Baron, A.T., and J.L. Salisbury. 1988. Identification and localization of a novel, cytoskeletal, centrosome-associated protein in PtK2 cells. *J Cell Biol*. 107:2669-2678.

Cho, K., M. Lee, D. Gu, W.A. Munoz, H. Ji, M. Kloc, and P.D. McCrea. 2011. Kazrin, and its binding partners ARVCF- and delta-catenin, are required for Xenopus laevis craniofacial development. *Developmental dynamics : an official publication of the American Association of Anatomists*. 240:2601-2612.

Cho, K., T.G. Vaught, H. Ji, D. Gu, C. Papasakelariou-Yared, N. Horstmann, J.M. Jennings, M. Lee, L.M. Sevilla, M. Kloc, A.B. Reynolds, F.M. Watt, R.G. Brennan, A.P. Kowalczyk, and P.D. McCrea. 2010. Xenopus Kazrin interacts with ARVCF-catenin, spectrin and p190B RhoGAP, and modulates RhoA activity and epithelial integrity. *J Cell Sci*. 123:4128-4144.

Driskell, O.J., A. Mironov, V.J. Allan, and P.G. Woodman. 2007. Dynein is required for receptor sorting and the morphogenesis of early endosomes. *Nat Cell Biol*. 9:113-120.

Flores-Rodriguez, N., S.S. Rogers, D.A. Kenwright, T.A. Waigh, P.G. Woodman, and V.J. Allan. 2011. Roles of dynein and dynactin in early endosome dynamics revealed using automated tracking and global analysis. *PLoS One*. 6:e24479.

Granger, E., G. McNee, V. Allan, and P. Woodman. 2014. The role of the cytoskeleton and molecular motors in endosomal dynamics. *Seminars in cell & developmental biology*. 31:20-29.

Grant, B.D., and S. Caplan. 2008. Mechanisms of EHD/RME-1 protein function in endocytic transport. *Traffic*. 9:2043-2052.

Groot, K.R., L.M. Sevilla, K. Nishi, T. DiColandrea, and F.M. Watt. 2004. Kazrin, a novel periplakin-interacting protein associated with desmosomes and the keratinocyte plasma membrane. *J Cell Biol*. 166:653-659.

Haberg, K., R. Lundmark, and S.R. Carlsson. 2008. SNX18 is an SNX9 paralog that acts as a membrane tubulator in AP-1-positive endosomal trafficking. *J Cell Sci*. 121:1495-1505.

Hsu, V.W., M. Bai, and J. Li. 2012. Getting active: protein sorting in endocytic recycling. *Nat Rev Mol Cell Biol*. 13:323-328.

Hunt, S.D., A.K. Townley, C.M. Danson, P.J. Cullen, and D.J. Stephens. 2013. Microtubule motors mediate endosomal sorting by maintaining functional domain organization. *J Cell Sci*. 126:2493-2501.

Jha, R., J. Roostalu, N.I. Cade, M. Trokter, and T. Surrey. 2017. Combinatorial regulation of the balance between dynein microtubule end accumulation and initiation of directed motility. *EMBO J*. 36:3387-3404.

Jones, M.C., P.T. Caswell, and J.C. Norman. 2006. Endocytic recycling pathways: emerging regulators of cell migration. *Curr Opin Cell Biol*. 18:549-557.

Kawauchi, T. 2012. Cell adhesion and its endocytic regulation in cell migration during neural development and cancer metastasis. *International journal of molecular sciences*. 13:4564-4590.

Kikuno, R., T. Nagase, K. Ishikawa, M. Hirosawa, N. Miyajima, A. Tanaka, H. Kotani, N. Nomura, and O. Ohara. 1999. Prediction of the coding sequences of unidentified human genes. XIV. The complete sequences of 100 new cDNA clones from brain which code for large proteins in vitro. *DNA research : an international journal for rapid publication of reports on genes and genomes*. 6:197-205.

Lee, I.G., S.E. Cason, S.S. Alqassim, E.L.F. Holzbaur, and R. Dominguez. 2020. A tunable LIC1-adaptor interaction modulates dynein activity in a cargo-specific manner. *Nat Commun*. 11:5695.

McNally, K.E., and P.J. Cullen. 2018. Endosomal Retrieval of Cargo: Retromer Is Not Alone. *Trends Cell Biol*. 28:807-822.

Nachat, R., S. Cipolat, L.M. Sevilla, M. Chhatriwala, K.R. Groot, and F.M. Watt. 2009. KazrinE is a desmosome-associated liprin that colocalises with acetylated microtubules. *J Cell Sci*. 122:4035-4041.

Naslavsky, N., and S. Caplan. 2018. The enigmatic endosome - sorting the ins and outs of endocytic trafficking. *J Cell Sci*. 131.

Naslavsky, N., J. Rahajeng, M. Sharma, M. Jovic, and S. Caplan. 2006. Interactions between EHD proteins and Rab11-FIP2: a role for EHD3 in early endosomal transport. *Mol Biol Cell*. 17:163-177.

Nielsen, E., F. Severin, J.M. Backer, A.A. Hyman, and M. Zerial. 1999. Rab5 regulates motility of early endosomes on microtubules. *Nat Cell Biol*. 1:376-382.

Perrin, L., S. Lacas-Gervais, J. Gilleron, F. Ceppo, F. Prodon, A. Benmerah, J.F. Tanti, and M. Cormont. 2013. Rab4b controls an early endosome sorting event by interacting with the gamma-subunit of the clathrin adaptor complex 1. *J Cell Sci*. 126:4950-4962.

Pollard, T.D., and B. O'Shaughnessy. 2019. Molecular Mechanism of Cytokinesis. *Annu Rev Biochem*. 88:661-689.

Prosser, S.L., and L. Pelletier. 2020. Centriolar satellite biogenesis and function in vertebrate cells. *J Cell Sci*. 133.

Sambrook, J., E.F. Fritsch, and T. Maniatis. 1989. Molecular Cloning: a Laboratory Manual, 2nd ed. . *Cold Spring Harbor Laboratory Press*.

Schmelzl, B., and M.I. Geli. 2002. An efficient genetic screen in mammalian cultured cells. *EMBO reports*. 3:682-687.

Sevilla, L.M., R. Nachat, K.R. Groot, and F.M. Watt. 2008a. Kazrin regulates keratinocyte cytoskeletal networks, intercellular junctions and differentiation. *J Cell Sci*. 121:3561-3569.

Sevilla, L.M., A.A. Rana, F.M. Watt, and J.C. Smith. 2008b. KazrinA is required for axial elongation and epidermal integrity in Xenopus tropicalis. *Developmental dynamics : an official publication of the American Association of Anatomists*. 237:1718-1725.

Sheff, D., L. Pelletier, C.B. O'Connell, G. Warren, and I. Mellman. 2002. Transferrin receptor recycling in the absence of perinuclear recycling endosomes. *J Cell Biol*. 156:797-804.

Solinger, J.A., H.O. Rashid, C. Prescianotto-Baschong, and A. Spang. 2020. FERARI is required for Rab11-dependent endocytic recycling. *Nat Cell Biol*. 22:213-224.

Szebenyi, G., B. Hall, R. Yu, A.I. Hashim, and H. Kramer. 2007. Hook2 localizes to the centrosome, binds directly to centriolin/CEP110 and contributes to centrosomal function. *Traffic*. 8:32-46.

Wang, H., W.T. Lo, and V. Haucke. 2019. Phosphoinositide switches in endocytosis and in the endolysosomal system. *Curr Opin Cell Biol*. 59:50-57.

Wang, Q., M. Liu, X. Li, L. Chen, and H. Tang. 2009. Kazrin F is involved in apoptosis and interacts with BAX and ARC. *Acta Biochim Biophys Sin (Shanghai)*. 41:763-772.

White, D.P., P.T. Caswell, and J.C. Norman. 2007. alpha v beta3 and alpha5beta1 integrin recycling pathways dictate downstream Rho kinase signaling to regulate persistent cell migration. *J Cell Biol*. 177:515-525.

Wilson, B.J., J.L. Allen, and P.T. Caswell. 2018. Vesicle trafficking pathways that direct cell migration in 3D matrices and in vivo. *Traffic*. 19:899-909.

Wilson, G.M., A.B. Fielding, G.C. Simon, X. Yu, P.D. Andrews, R.S. Hames, A.M. Frey, A.A. Peden, G.W. Gould, and R. Prekeris. 2005. The FIP3-Rab11 protein complex regulates recycling endosome targeting to the cleavage furrow during late cytokinesis. *Mol Biol Cell*. 16:849-860.

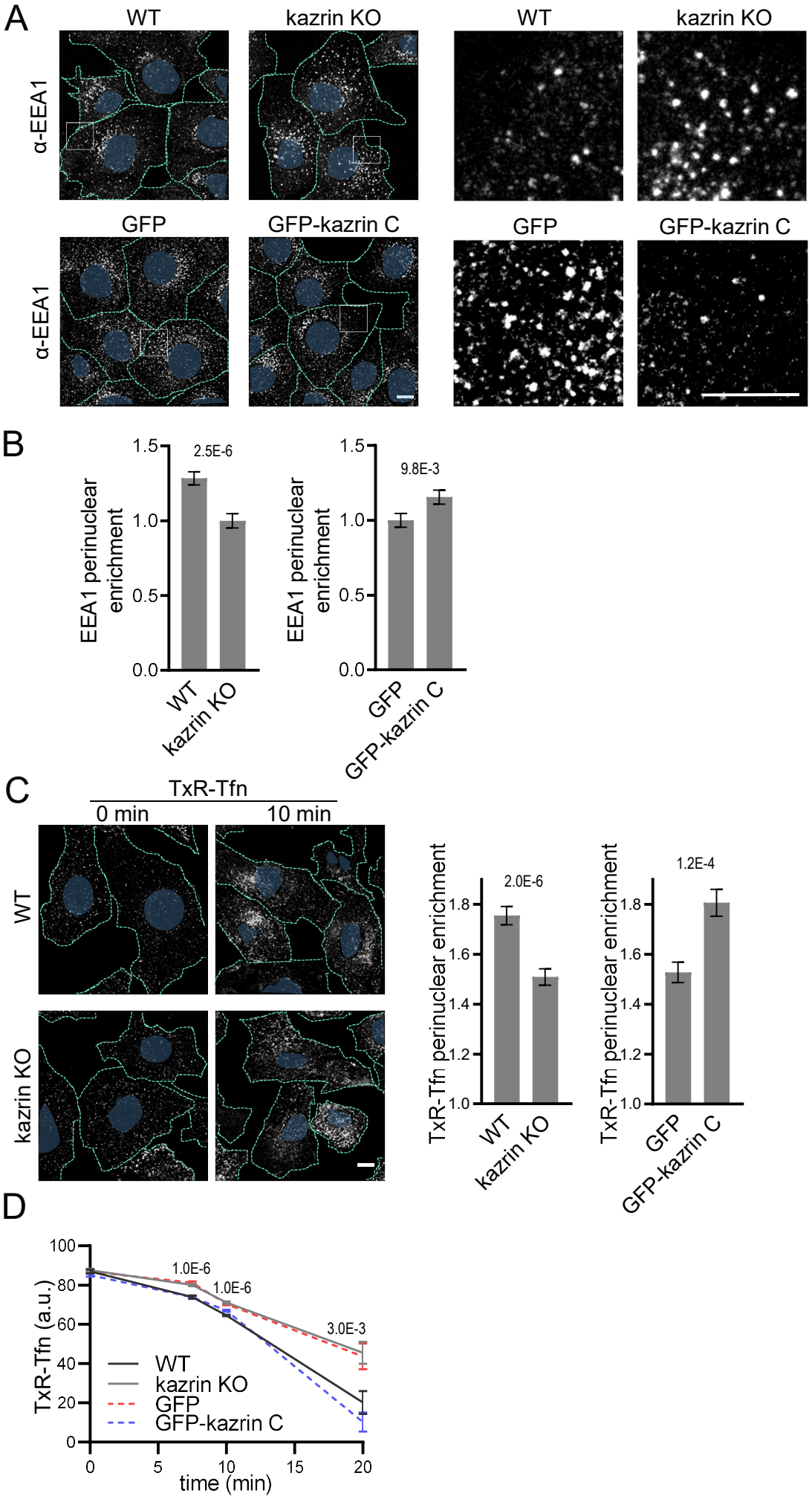
A
WT
kazrin KO
WT
kazrin KO
α-EEA1
GFP
GFP-kazrin C
GFP
GFP-kazrin C
α-EEA1
B
EEA1 perinuclear enrichment
1.5
1.0
0.5
0.0
2.5E-6
WT
kazrin KO
EEA1 perinuclear enrichment
1.5
1.0
0.5
0.0
9.8E-3
GFP
GFP-kazrin C
C
TxR-Tfn
0 min
10 min
WT
kazrin KO
TxR-Tfn perinuclear enrichment
1.8
1.6
1.4
1.2
1.0
2.0E-6
WT
kazrin KO
TxR-Tfn perinuclear enrichment
1.8
1.6
1.4
1.2
1.0
1.2E-4
GFP
GFP-kazrin C
D
TxR-Tfn (a.u.)
100
80
60
40
20
0
1.0E-6
1.0E-6
3.0E-3
WT
kazrin KO
GFP
GFP-kazrin C
0
5
10
15
20
time (min)

Fig. 1

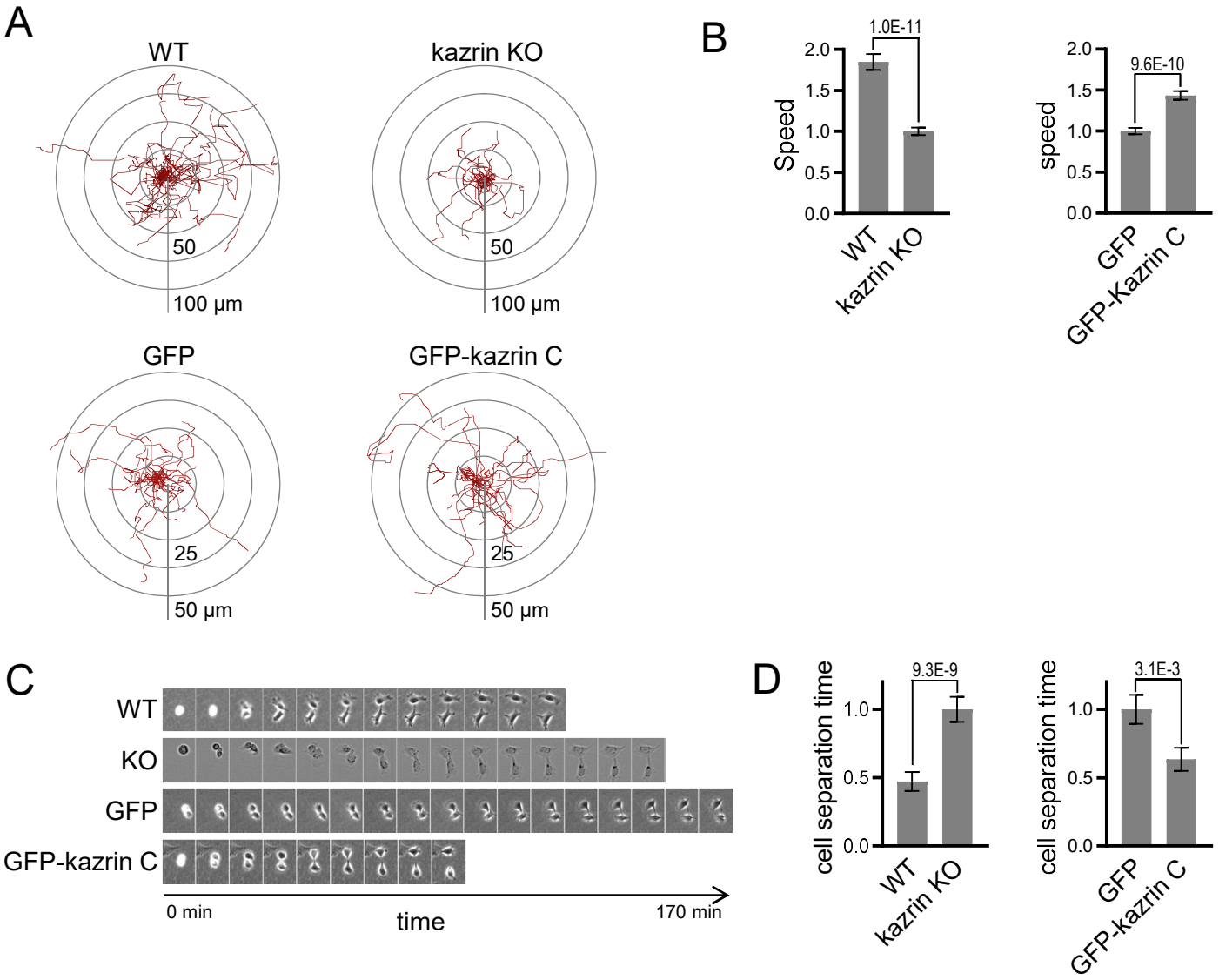
A
WT
kazrin KO
50
100 μm
50
100 μm
GFP
GFP-kazrin C
25
50 μm
25
50 μm
B
1.0E-11
Speed
2.0
1.5
1.0
0.5
0.0
WT
kazrin KO
9.6E-10
speed
2.0
1.5
1.0
0.5
0.0
GFP
GFP-kazrin C
C
WT
KO
GFP
GFP-kazrin C
0 min
time
170 min
D
9.3E-9
cell separation time
1.0
0.5
0.0
WT
kazrin KO
3.1E-3
cell separation time
1.0
0.5
0.0
GFP
GFP-kazrin C

Fig. 2

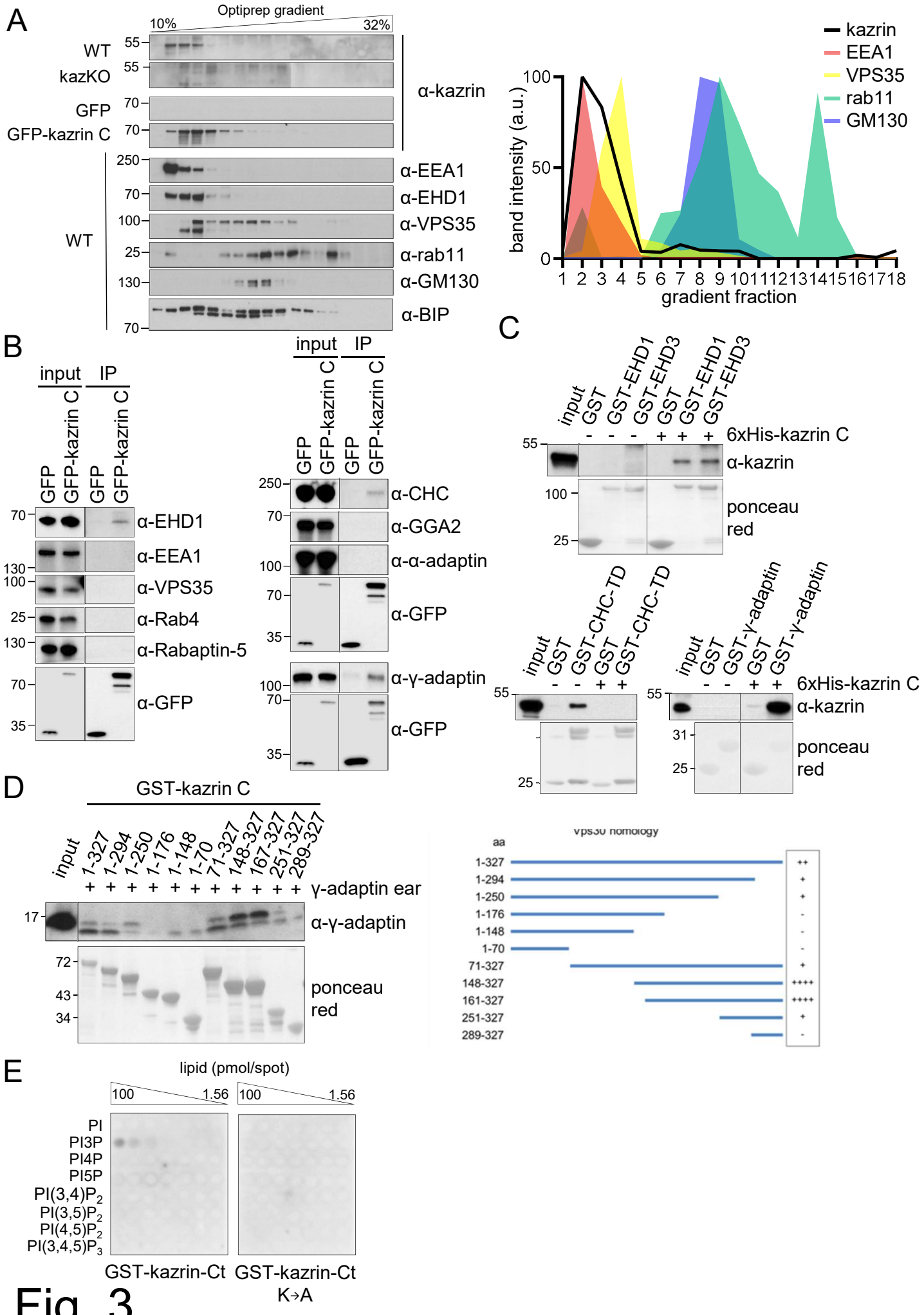
A
Optiprep gradient
10%
32%
WT
kazKO
GFP
GFP-kazrin C
α-kazrin
α-EEA1
α-EHD1
α-VPS35
α-rab11
α-GM130
α-BIP
kazrin
EEA1
VPS35
rab11
GM130
band intensity (a.u.)
gradient fraction
B
input
IP
GFP
GFP-kazrin C
α-EHD1
α-EEA1
α-VPS35
α-Rab4
α-Rabaptin-5
α-GFP
α-CHC
α-GGA2
α-α-adaptin
α-γ-adaptin
C
input
GST
GST-EHD1
GST-EHD3
6xHis-kazrin C
α-kazrin
ponceau red
GST-CHC-TD
GST-γ-adaptin
D
GST-kazrin C
1-327
1-294
1-250
1-176
1-148
1-70
71-327
148-327
167-327
251-327
289-327
γ-adaptin ear
α-γ-adaptin
ponceau red
vps30 homology
aa
E
lipid (pmol/spot)
100
1.56
PI
PI3P
PI4P
PI5P
PI(3,4)P2
PI(3,5)P2
PI(4,5)P2
PI(3,4,5)P3
GST-kazrin-Ct
GST-kazrin-Ct K→A

Fig. 3

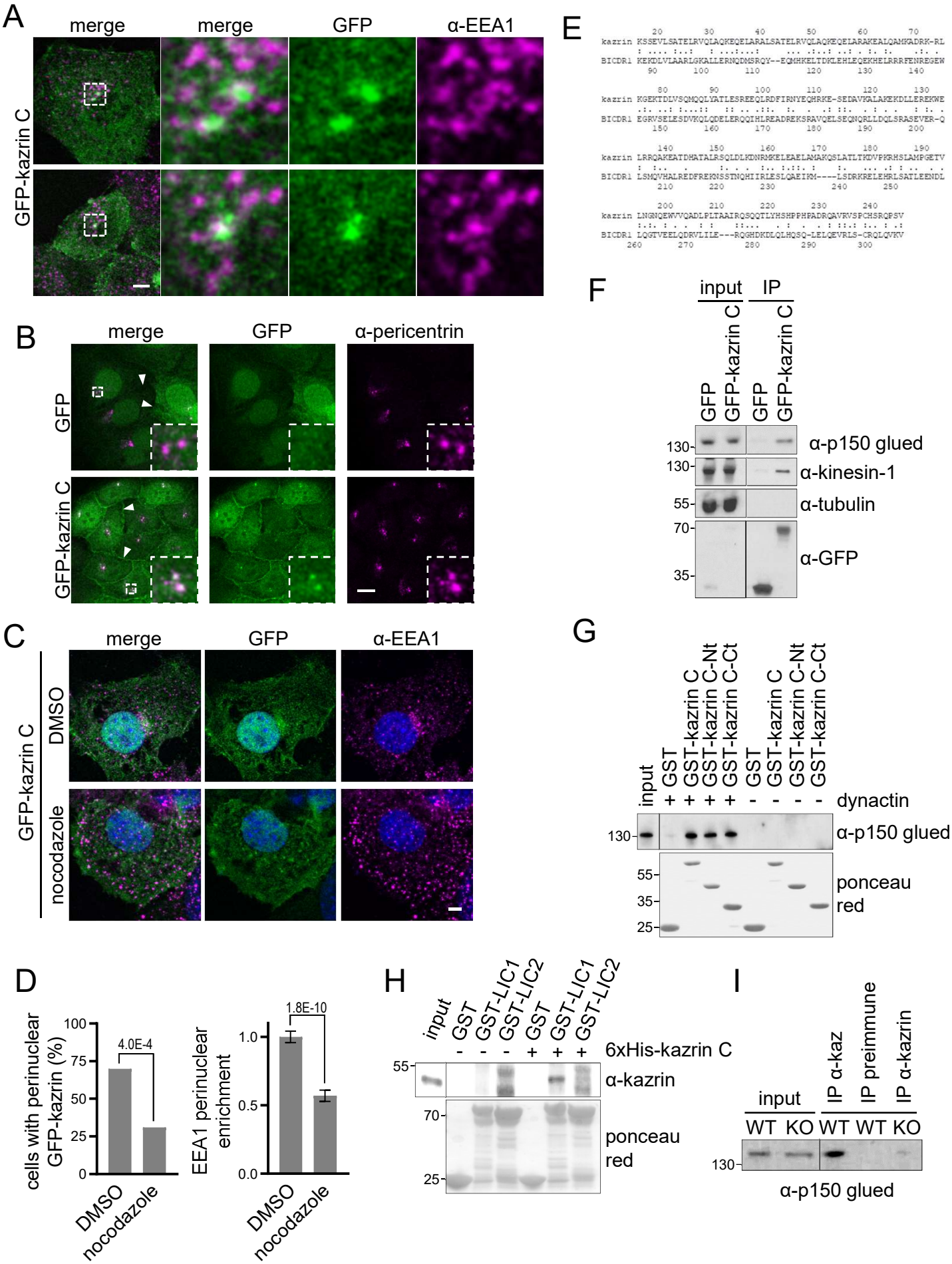
A
merge
merge
GFP
α-EEA1
GFP-kazrin C
B
merge
GFP
α-pericentrin
GFP
GFP-kazrin C
C
merge
GFP
α-EEA1
GFP-kazrin C
DMSO
nocodazole
D
cells with perinuclear GFP-kazrin (%)
4.0E-4
DMSO
nocodazole
EEA1 perinuclear enrichment
1.8E-10
DMSO
nocodazole
E
kazrin
BICDR1
F
input
IP
GFP
GFP-kazrin C
GFP
GFP-kazrin C
130
α-p150 glued
130
α-kinesin-1
55
α-tubulin
70
35
α-GFP
G
input
GST
GST-kazrin C
GST-kazrin C-Nt
GST-kazrin C-Ct
GST
GST-kazrin C
GST-kazrin C-Nt
GST-kazrin C-Ct
dynactin
130
α-p150 glued
55
35
25
ponceau red
H
input
GST
GST-LIC1
GST-LIC2
GST
GST-LIC1
GST-LIC2
6xHis-kazrin C
55
α-kazrin
70
25
ponceau red
I
input
IP α-kaz
IP preimmune
IP α-kazrin
WT
KO
WT
WT
KO
130
α-p150 glued

Fig. 4